Letters

Enhanced Excitation Converter With Parallel/Series DC-Link Based on TAB for DFIG to Improve the LVRT Capability Under Severe Grid Faults

Jiateng Gu, Rende Zhao, *Member, IEEE*, Jinkui He, Juntao Xu, Qingzeng Yan, Chuandong Sun, and Hao Liu

***Abstract*—The low-voltage ride-through (LVRT) capability of the doubly-fed induction generator (DFIG) based on the conventional excitation converter is insufficient under severe grid faults. The reason is that the dynamic rotor electromotive forces (EMF) will far exceed the dc-link voltage. To solve this issue, this letter proposes an enhanced excitation converter with parallel/series dc-link based on the triple active bridge (TAB) for DFIG. The dc-link of the enhanced excitation converter consists of the TAB and switching circuit, replacing the capacitive-type dc-link. Based on this topology, the dc-link voltage can increase instantaneously during severe grid faults to resist rotor EMF and improve the LVRT capability of DFIG. Compared with existing LVRT schemes, the enhanced excitation converter enables DFIG to achieve LVRT and inject the reactive current requirements of the grid code into the grid under severe grid faults. Finally, experiments verified the effectiveness of the proposed enhanced excitation converter and its control strategy.**

***Index Terms*—Doubly-fed induction generator (DFIG), enhanced excitation converter, low-voltage ride-through (LVRT).**

I. Introduction

With the increasing penetration of wind power, grid-connected wind turbines (WTs) must have excellent low-voltage ride-through (LVRT) capability. During grid faults, WTs must remain connected to the grid and inject reactive currents into the grid according to the grid code [1]. The doubly-fed induction generator (DFIG)-based WT is the mainstream type of onshore wind energy conversion system [2]. Unfortunately, the LVRT capability of the DFIG based on the conventional excitation converter is insufficient under severe grid faults, as the rotor electromotive forces (EMF) will far exceed the dc-link voltage.

The various LVRT schemes proposed in previous literature are mainly classified into auxiliary hardware (including modifying the excitation converter) and improving the rotor-side converter (RSC) control strategies. Several schemes for modification of the control strategy of RSC have been proposed to improve the LVRT capability of the DFIG [3], [4], [5]. The schemes, however, cannot meet grid code requirements under severe grid faults due to the capacity limitation of RSC. The auxiliary hardware scheme has been considered useful in improving the LVRT capability of DFIG under severe grid faults. The crowbar protection scheme is the most widely used auxiliary hardware scheme [6]. Nevertheless, the application of the crowbar will cause the DFIG to operate as an induction generator. This will result in DFIG losing controllability and absorbing rather than injecting reactive current from the grid. Dynamic voltage restorer was proposed to compensate for the stator voltage under grid faults [7]. However, the scheme requires a full-rated series transformer. The fault current limiter was proposed to limit fault current in [8]. Unfortunately, the reactive current injection capability of DFIG was also limited.

To meet grid code requirements under severe grid faults, some researchers have tried to modify the excitation converter directly. In [9], a nine-switch converter was applied to DFIG as the excitation converter. Although this structure can improve the LVRT capability under severe grid faults, it can only be used in step-down DFIG. In [10], a novel RSC topology based on H-bridge was proposed to improve the LVRT capability of DFIG under severe grid faults. But the volume and cost of the novel RSC topology cannot be ignored.

This letter proposed an enhanced excitation converter with parallel/series dc-link based on the triple active bridge (TAB) for DFIG to improve its LVRT capability under severe grid faults. Based on the enhanced excitation converter, DFIG cannot only maintain grid-connected operation under severe grid faults but also inject reactive currents into the grid according to grid code requirements.

Manuscript received 3 April 2023; revised 13 May 2023; accepted 8 June 2023. Date of publication 13 June 2023; date of current version 1 September 2023. This work was supported by the National Natural Science Foundations of China under Grant 52177203. *(Corresponding author: Rende Zhao.)*

Jiateng Gu, Rende Zhao, Jinkui He, and Qingzeng Yan are with the College of New Energy, China University of Petroleum (East China), Qingdao 266580, China (e-mail: gjt201218@163.com; zhaorende@upc.edu.cn; hjk@upc.edu.cn; yqz2009@163.com).

Juntao Xu is with the College of New Energy, China University of Petroleum (East China), Qingdao 266580, China, and also with the Shandong Electric Power Engineering Consulting Institute Company, Ltd, Jinan 250013, China (e-mail: 333xujuntao@163.com).

Chuandong Sun is with the State Grid Linfen Power Supply Company, Linfen 041000, China (e-mail: scd1008@qq.com).

Hao Liu is with the Linyi Power Supply Company, State Grid Shandong Electric Power Company, Linyi 276000, China (e-mail: liuhaoupc@163.com).

Color versions of one or more figures in this article are available at https://doi.org/10.1109/TPEL.2023.3285900.

Digital Object Identifier 10.1109/TPEL.2023.3285900

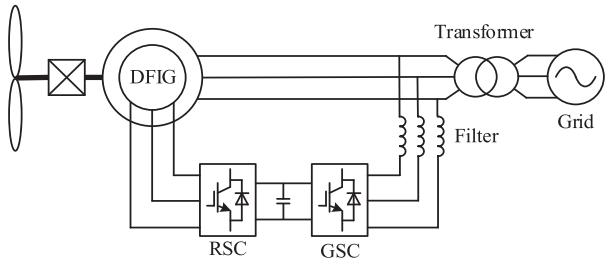

Fig. 1. Topology of DFIG-based WT based on the conventional excitation converter.

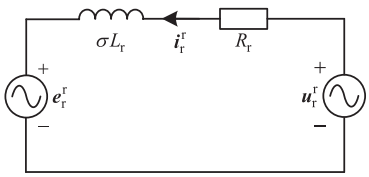

Fig. 2. Equivalent circuit of DFIG in the rotor reference frame.

II. Bottlenecks Analysis of Conventional Excitation Converter

The topology of DFIG-based WT based on the conventional excitation converter is shown in Fig.1. The RSC and grid side converter (GSC) are connected via a capacitive-type dc-link. In the static rotor reference frame, the DFIG equivalent circuit from the rotor side is shown in Fig. 2. The rotor voltage space phasor with the Park model can be expressed as [11]

$$\begin{cases} \boldsymbol{u}_{\mathrm{r}}^{\mathrm{r}} = \boldsymbol{e}_{\mathrm{r}}^{\mathrm{r}} + R_{\mathrm{r}}\boldsymbol{i}_{\mathrm{r}}^{\mathrm{r}} + \sigma L_{\mathrm{r}}\frac{d\boldsymbol{i}_{\mathrm{r}}^{\mathrm{r}}}{dt} \\ \boldsymbol{e}_{\mathrm{r}}^{\mathrm{r}} = k_{ms}(\frac{d}{dt} - j\omega_r)\boldsymbol{\psi}_s^r = k_{ms}sU_{sm}e^{js\omega_1 t} \end{cases} \tag{1}$$

where $\boldsymbol{u}_{\mathrm{r}}^{\mathrm{r}}$ is the rotor voltage space phasor, $\boldsymbol{e}_{\mathrm{r}}^{\mathrm{r}}$ is the rotor EMF space phasor, $\boldsymbol{i}_{\mathrm{r}}^{\mathrm{r}}$ is the rotor current space phasor, R_{r} is the rotor resistance, $\sigma = 1 - L_{\mathrm{m}}^2/L_{\mathrm{s}}L_{\mathrm{r}}$ is the leakage coefficient, L_{m} is the mutual inductance, L_{s} is the stator inductance, L_{r} is the rotor inductance, $k_{\mathrm{ms}} = L_{\mathrm{m}}/L_{\mathrm{s}}$ is the excitation coefficient, $\boldsymbol{\psi}_{\mathrm{s}}^{\mathrm{r}}$is stator flux space phasor, s is the slip, U_{sm} is the amplitude of stator voltage, and ω_1 is the grid angular frequency. The superscript "r" represents the rotor reference frame.

The rotor EMF space phasor with the Park model in the rotor reference frame under pre- and post-symmetric faults can be expressed as [11]

$$\begin{cases} \boldsymbol{e}_{\mathrm{r1}}^{\mathrm{r}} = k_{ms}sU_{\mathrm{sm1}}e^{js\omega_1 t}, t < t_0 \\ \boldsymbol{e}_{\mathrm{r2}}^{\mathrm{r}} = k_{ms}[sU_{\mathrm{sm2}}e^{js\omega_1 t} - (1-s)(U_{\mathrm{sm1}} \\ \qquad -U_{\mathrm{sm2}})e^{-j\omega_{\mathrm{r}}t}e^{-(t-t_0)/\tau_{\mathrm{s}}}], t \geq t_0 \end{cases} \tag{2}$$

where $\boldsymbol{e}_{\mathrm{r1}}^{\mathrm{r}}$ and $\boldsymbol{e}_{\mathrm{r2}}^{\mathrm{r}}$ are the rotor EMF space phasor under pre- and post-symmetric faults, U_{sm1} and U_{sm2} are the amplitude of pre- and post-symmetric faults stator voltage, ω_{r} is the rotor angular frequency, τ_{s} is the stator time constant, and t_0 is the faults time.

According to (2), the maximum amplitude of the EMF under normal conditions is $0.3U_{\mathrm{s}}$, due to $L_{\mathrm{m}}/L_{\mathrm{s}} \approx 1$ and $s \in [-0.3, 0.3]$. Thus, the dc-link voltage of the conventional excitation converter is usually set at $0.5U_{\mathrm{s}}$ [12]. However, the amplitude of the rotor EMF under the post-symmetric fault will suddenly increase to $1.1U_{\mathrm{s}}$ in the severe conditions of $s = -0.3$ and $U_{\mathrm{sm2}} = 0.2U_{\mathrm{sm1}}$, which far exceeds the dc-link voltage, as shown in Fig. 3. The DFIG will suffer from overcurrent due to high EMF and cannot achieve LVRT.

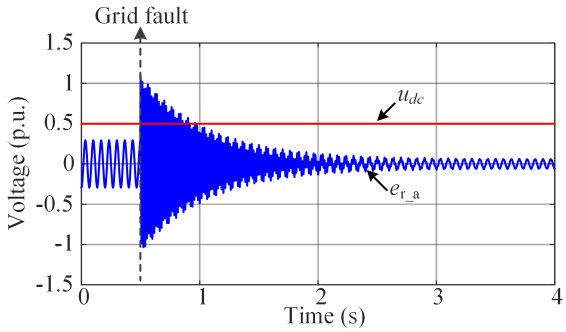

Fig. 3. EMF and DC-link voltage of pre- and post-symmetric faults based on the conventional excitation converter.

The reason for the insufficient LVRT capability of DFIG based on a conventional excitation converter is that the EMF far exceeds the dc-link voltage under severe grid faults. Therefore, the direct way to improve the LVRT capability of DFIG is to design a new excitation converter to increase the dc-link voltage under severe grid faults. However, the higher dc-link voltage will affect the operation of DFIG during normal conditions. On the one hand, the higher dc-link voltage will aggravate the effect of dead time when the output voltage of RSC is low, affecting the quality of DFIG power generation. On the other hand, the higher dc-link voltage will produce a larger *dv/dt*, leading to a larger EMI.

To solve the abovementioned problem, this letter presents an enhanced excitation converter based on a new dc-link topology for DFIG. In the enhanced excitation converter, the dc-link voltage can be held at a low level during normal conditions to improve DFIG power generation quality. When severe grid faults occur, the dc-link voltage of the enhanced excitation converter can rise instantaneously to help DFIG achieve LVRT.

III. Topology and Control Strategy of Enhanced Excitation Converter

A. Topology of Enhanced Excitation Converter

The topology of the proposed enhanced excitation converter is shown in Fig. 4, which consists of GSC, RSC, and parallel/series dc-link based on TAB. The GSC and RSC adopt a two-level converter and a three-level neutral-point clamped converter, respectively. The parallel/series dc-link replaces the capacitive-type dc-link in a conventional excitation converter, which can instantaneously increase the dc-link voltage under severe grid faults.

Concretely, the parallel/series dc-link is composed of the TAB converter and the series-parallel switching circuit. TAB is used to achieve electrical isolation and variable voltage. The output voltage of TAB is set to half of the GSC output voltage, i.e., $v_1 = 0.5v_{\mathrm{in}}$. The function of the series-parallel switching circuit is to control the parallel or series operation of TAB output terminals

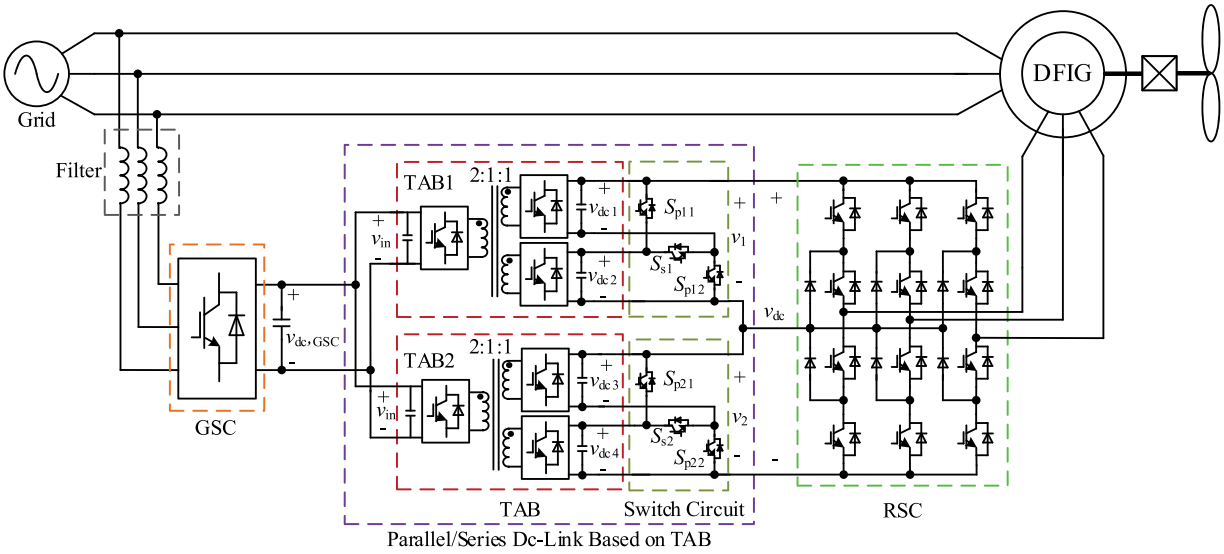

Fig. 4. Topology of the enhanced excitation converter with parallel/series DC-link based on TAB for DFIG.

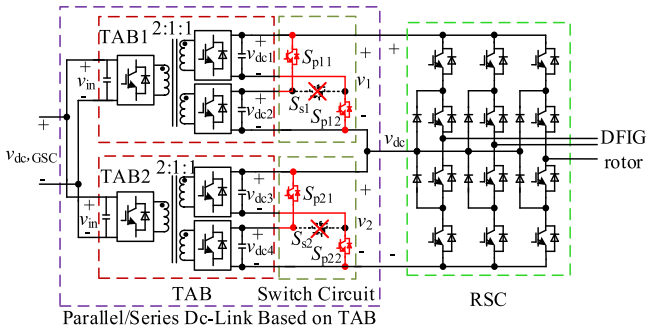

Fig. 5. Connection parallel/series DC-link in normal conditions.

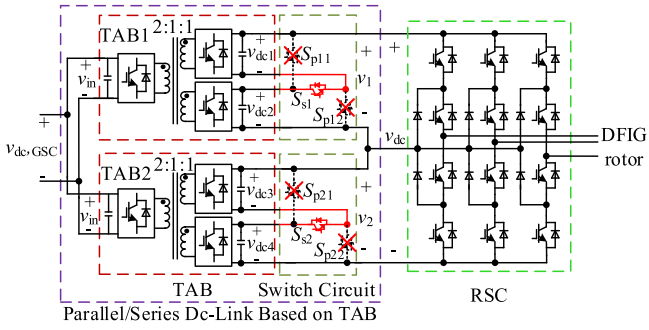

Fig. 6. Connection parallel/series DC-link in fault conditions.

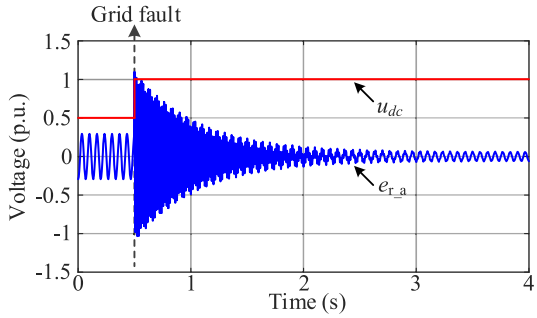

Fig. 7. EMF and DC-link voltage of pre- and post-symmetric faults based on the enhanced excitation converter.

to realize the state switching of dc-link voltage. In normal conditions, S_{p11}, S_{p12}, S_{p21}, and S_{p22} are set to turn ON, while S_{s1} and S_{s2} are set to turn OFF, as shown in Fig. 5. In this condition, TAB output terminals are paralleled together. The dc-link voltage $v_{dc} = v_{dc1}$ is at a normal level to ensure high-quality DFIG power generation. When severe grid faults occur, S_{p11}, S_{p12}, S_{p21}, and S_{p22} are set to turn OFF, while S_{s1} and S_{s2} are set to turn ON, as shown in Fig. 6. In this condition, TAB output terminals are switched from parallel to series operation. As a result, the dc-link voltage doubles instantaneously compared with normal conditions, as shown in Fig. 7. The higher dc-link voltage can improve the output voltage of RSC to resist rotor EMF and help DFIG achieve LVRT.

B. Control Strategy of Enhanced Excitation Converter

To achieve LVRT, the LVRT control strategy of DFIG based on the enhanced excitation converter should be designed. For the enhanced excitation converter, the GSC control strategy is the same as the traditional excitation converter, which was not described in this letter. The control structure diagram of dc-link and RSC is shown in Fig. 8. The single-phase-shift-based output voltage feedback control was adopted in TAB at any conditions to maintain the better performance of output voltage stability and dynamic response [13]. The faults detection module detects the grid state in real time by collecting the grid voltage. In this letter, the amplitude of the grid voltage u_{sd} was collected in real time to detect grid faults. When $U_{sd} \leq 0.9U_{sN}$ was detected, we assumed the grid fault was occurring. Then, the control system mode was switched from the normal state to the fault state. The working mode of the switch circuit control module and RSC

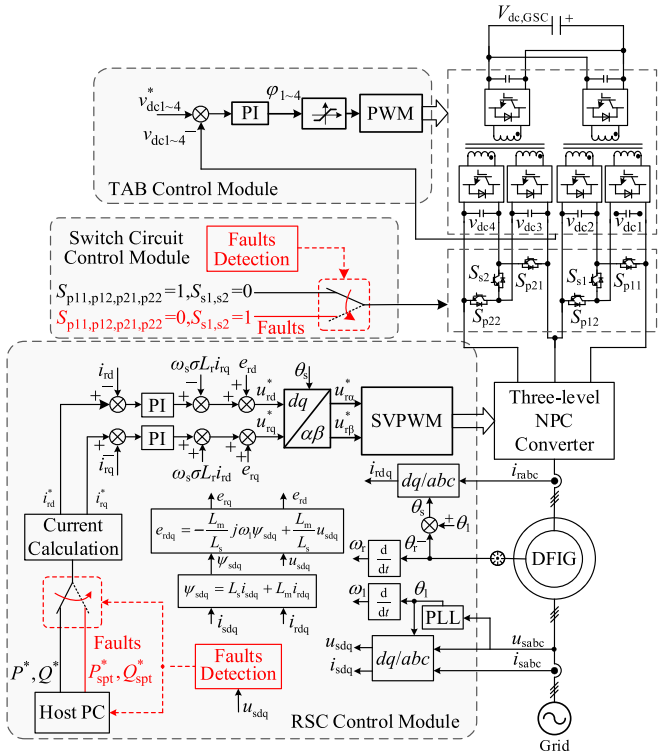

Fig. 8. Control structure diagram of DC-link and RSC.

TABLE I
PARAMETERS OF THE DFIG PROTOTYPE

Parameter	Value	Parameter	Value
Rated power	1.5 kW	Stator resistance	1.1 Ω
Rated frequency	50 Hz	Stator leakage inductance	6.0 mH
Rated stator voltage	220 V	Rotor resistance	2.3 Ω
Turn ratio	1:1.66	Rotor leakage inductance	6.0 mH
Pairs of poles	3	Mutual inductance	123 mH

control module is based on the detection results of the faults detection module. The control strategy of RSC adopts the power open loop and the current closed loop.

Under normal conditions, the active power command is the rated power of DFIG, and the reactive power command is 0.

The TAB output terminals are paralleled together with the switch circuit control module control. When the faults detection module detects the grid voltage below 0.9 per unit (p.u.), the output terminals of TAB instantaneously switch from parallel to series operation to improve the dc-link voltage and help DFIG achieve LVRT. Meanwhile, the host PC sends reactive power instructions to the DFIG so that the DFIG can inject the required reactive current according to the grid code.

IV. Experiment Verification

The effectiveness of the proposed enhanced excitation converter with parallel/series dc-link based on TAB for DFIG has been verified with a 1.5 kW DFIG-based WT prototype. The prototype schematic diagram is shown in Fig. 9, and the parameters of DFIG are given in Table I. Under normal grid conditions,

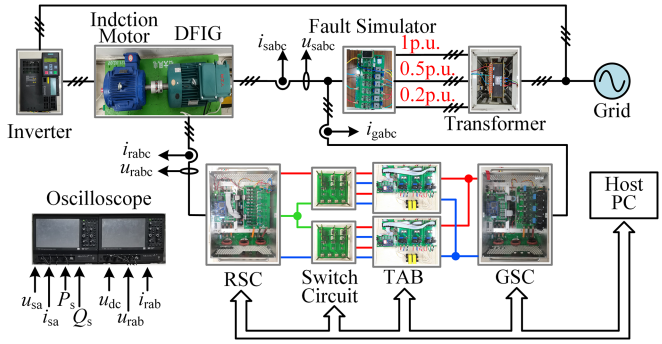

Fig. 9. Schematic diagram of the experimental setup.

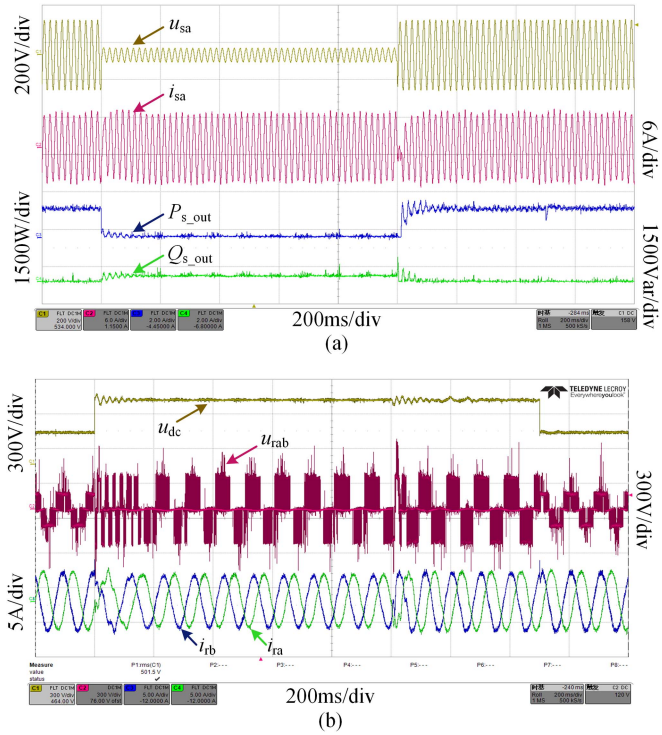

Fig. 10. LVRT experimental results for an 80% symmetrical grid fault. (a) DFIG stator voltage, current, and output power waveforms. (b) DFIG rotor current, voltage, and DC-link voltage waveforms.

DFIG operates in a stable state. The rotor speed was set at 1.2 p.u. and remained constant during grid faults. The active power and reactive power of DFIG output are controlled at 1.5 kW and 0 Var, respectively.

Figs. 10 and 11 show the LVRT experimental results for an 80% symmetrical grid fault. When grid fault was detected, the dc-link voltage u_{dc} doubled instantaneously to increase RSC output voltage. The active power was set at 0 W, and the reactive power was set at 315 Var to satisfy the grid code requirement. After the grid fault was cleared, the active power was reset at 1500 W, and the reactive power was reset at 0 Var. The dc-link voltage remains high level for a certain period to help the DFIG recover. When the DFIG is restable, the dc-link voltage returns to the normal level. According to Fig. 11(b), the rotor overcurrent was effectively suppressed in both conditions of grid fault and

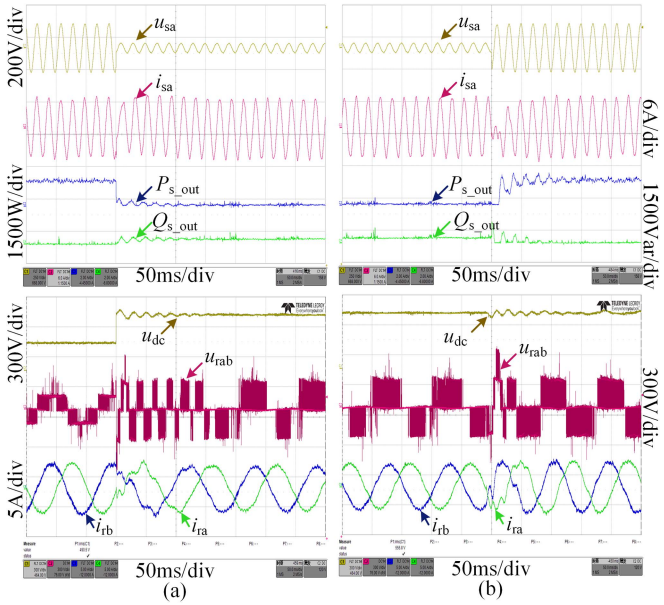

Fig. 11. Amplification diagram of LVRT experimental results for an 80% symmetrical fault. (a) Grid fault. (b) Grid recovery.

grid recovery, and LVRT was achieved. From Fig. 11(a), it can be seen that DFIG injects the reactive current required by the grid code into the grid under the grid fault. The stator current increased to 5.9 A (1.05 p.u.) from 5.6 A (1 p.u.).

V. Conclusion

In this letter, an enhanced excitation converter with parallel/series dc-link based on TAB for DFIG has been proposed to improve the LVRT capability of DFIG under severe grid faults. Experimental tests have verified the effectiveness of the proposed enhanced excitation converter. It shows that the enhanced excitation converter can improve the LVRT capability of DFIG under severe grid faults. With the enhanced excitation converter, DFIG can not only remain connected to the grid but also inject the reactive current required by the grid code under severe grid faults.

References

[1] Y. Yang, D. Zhu, X. Zou, Y. Chi, and Y. Kang, "Power compensation control for DFIG-based wind turbines to enhance synchronization stability during severe grid faults," *IEEE Trans. Power Electron.*, vol. 37, no. 9, pp. 10139–10143, Sep. 2022.

[2] T. Zhang et al., "Improved continuous fault ride through control strategy of DFIG-based wind turbine during commutation failure in the LCC-HVDC transmission system," *IEEE Trans. Power Electron.*, vol. 36, no. 1, pp. 459–473, Jan. 2021.

[3] D. Zhou and F. Blaabjerg, "Optimized demagnetizing control of DFIG power converter for reduced thermal stress during symmetrical grid fault," *IEEE Trans. Power Electron.*, vol. 33, no. 12, pp. 10326–10340, Dec. 2018.

[4] Z. Rafiee, R. Heydari, M. Rafiee, M. R. Aghamohammadi, and F. Blaabjerg, "Enhancement of the LVRT capability for DFIG-based wind farms based on short-circuit capacity," *IEEE Syst. J.*, vol. 16, no. 2, pp. 3237–3248, Jun. 2022.

[5] D. Zhu, X. Zou, L. Deng, Q. Huang, S. Zhou, and Y. Kang, "Inductance-emulating control for DFIG-based wind turbine to ride-through grid faults," *IEEE Trans. Power Electron.*, vol. 32, no. 11, pp. 8514–8525, Nov. 2017.

[6] A. M. A. Haidar, K. M. Muttaqi, and M. T. Hagh, "A coordinated control approach for dc link and rotor crowbars to improve fault ride-through of DFIG-based wind turbine," *IEEE Trans. Ind. Appl.*, vol. 53, no. 4, pp. 4073–4086, Jul./Aug. 2017.

[7] R. H. Yang and J. X. Jin, "Unified power quality conditioner with advanced dual control for performance improvement of DFIG-based wind farm," *IEEE Trans. Sustain. Energy*, vol. 12, no. 1, pp. 116–126, Jan. 2021.

[8] M. Firouzi and G. B. Gharehpetian, "LVRT performance enhancement of DFIG-based wind farms by capacitive bridge-type fault current limiter," *IEEE Trans. Sustain. Energy*, vol. 9, no. 3, pp. 1118–1125, Jul. 2018.

[9] G. Wen, Y. Chen, Z. Zhong, and Y. Kang, "Dynamic voltage and current assignment strategies of nine-switch-converter-based DFIG wind power system for low-voltage ride-through (LVRT) under symmetrical grid voltage dip," *IEEE Trans. Ind. Appl.*, vol. 52, no. 4, pp. 3422–3434, Jul./Aug. 2016.

[10] C. Meng, R. Zhao, C. Yuan, and C. Xuan, "A novel rotor-side converter topology of doubly-fed wind turbine based on H-bridge," in *Proc. IEEE 1st China Int. Youth Conf. Elect. Eng.*, 2020, pp. 1–5.

[11] J. Lopez, P. Sanchis, X. Roboam, and L. Marroyo, "Dynamic behavior of the doubly fed induction generator during three-phase voltage dips," *IEEE Trans. Energy Convers.*, vol. 22, no. 3, pp. 709–717, Sep. 2007.

[12] X. Zou, D. Zhu, J. Hu, S. Zhou, and Y. Kang, "Mechanism analysis of the required rotor current and voltage for DFIG-based WTs to ride-through severe symmetrical grid faults," *IEEE Trans. Power Electron.*, vol. 33, no. 9, pp. 7300–7304, Sep. 2018.

[13] S. Shao et al., "Modeling and advanced control of dual-active-bridge DC-DC converters: A review," *IEEE Trans. Power Electron.*, vol. 37, no. 2, pp. 1524–1547, Feb. 2022.